arXiv:1603.07549v1 [math.NA] 23 Mar 2016

Application of the Finite Element Method in a Quantitative Imaging technique

L. Beilina *

Abstract

We present the Finite Element Method (FEM) for the numerical solution of the multi-dimensional coefficient inverse problem (MCIP) in two dimensions. This method is used for explicit reconstruction of the coefficient in the hyperbolic equation using data resulted from a single measurement. To solve our MCIP we use approximate globally convergent method and then apply FEM for the resulted equation. Our numerical examples show quantitative reconstruction of the sound speed in small tumor-like inclusions.

1 Introduction

In this work we present the Finite Element Method (FEM) applied for explicit reconstruction of the coefficient in the hyperbolic equation using data resulted from a single measurement. This means that the data are generated by either a single location of the point source or by a single direction of the incident plane wave. Such multidimensional coefficient inverse problems (MCIPs) are non-overdetermined ones and have a lot of applications, such as, e.g., many aspects of acoustics, electromagnetics, optics, medical imaging, geophysics, etc..

To solve our MCIP we use approximate globally convergent method of [5] where for the solution of MCIP was used underlying PDE operator instead of least squares functionals. It is well known that CIPs are both nonlinear and ill-posed. A main idea of an approximate globally convergent method is that the least squares objective functionals are not used in it and the phenomenon of local minima is avoided. This method was further verified on computationally simulated and on experimental data in [6–8, 10] and references therein.

In the current work we apply the finite element method inside approximate globally convergent method of [5]. Our goal is obtain quantitative medical imaging of small inclusions representing cancerous tumors. This means that we are interested not only in shape reconstruction but also in the accurate reconstruction of the contrast of tumor-like inclusions. Examples of MCIPs with applications in medicine are inverse problems of magnetic resonance elastography (MRE) which are studied recently in [2, 11] and references therein. The main feature of this medical imaging technique is that it allows measure field internally and this is the case of our numerical examples of section 6. We note that for detection of cancer tumors in human tissue using MRE technique stiffness contrast can be of the order of 2000% while the density varies only of the order of 8% [11]. This is the main reason why stiffness is diagnostically more useful and density is often not considered.

The current work is devoted to the reconstruction of the wave speed in the wave equation from internal measurements. We consider the simplified model problem described by the acoustic

*Department of Mathematical Sciences, Chalmers University of Technology and Gothenburg University, SE-42196 Gothenburg, Sweden, e-mail: larisa@chalmers.se

wave equation instead of the elastic one. Application of the method of this work for another MCIPs can be considered as a topic for a future research. Numerical examples of section 6 show very accurate and quantitative reconstruction of tumor-like inclusions which can be even of the very small sizes (point-size inclusions). In our future work we plan to extend the iterative procedure described in this work to the case of MCIPs with boundary measurements. Similarly with [1] an adaptive finite element method can be also considered as a topic for a future research.

2 Statements of Forward and Inverse Problems

We consider the Cauchy problem for the hyperbolic equation

$$a(x)u_{tt} = \Delta u \text{ in } \mathbb{R}^3 \times (0,\infty), \tag{1}$$

$$u(x,0) = 0,\ u_t(x,0) = \delta(x - x_0), \tag{2}$$

where δ is the Dirac delta function. Equation (1) governs a wide range of applications, including, e.g. propagation of acoustic, elastic and electromagnetic waves. In the acoustical case $c(x) = 1/\sqrt{a(x)}$ is the sound speed. In the electromagnetic waves propagation in a non-magnetic medium, the dimensionless coefficient is $a(x) = \varepsilon_r(x)$, where $\varepsilon_r(x)$ is the spatially distributed dielectric constant of the medium. In the case of application of equation (1) in scanning acoustic microscopy in medical imaging, the sound speed is defined as $c(x) = \sqrt{(\lambda(x) + 2\mu(x))/\rho(x)}$, where $\rho(x)$ is the density and $\lambda(x), \mu(x)$ are the Lamé constants of linear elasticity [4]. In the current paper we consider this kind of applications when the function $a(x)$ in (1) can be determined as $a(x) = \rho(x)/(\lambda(x) + 2\mu(x))$. Then by the reconstructed function $a(x)$ it will be possible determine the stiffness coefficient $\mu(x)$ for the known functions $\rho(x), \lambda(x)$.

Let $\Omega \subset \mathbb{R}^3$ be a convex bounded domain with the boundary $\partial\Omega \in C^3$. Let $d = const. > 1$. We assume that the coefficient $a(x)$ of equation (1) is such that

$$a(x) \in [1,d],\quad a(x) = 1 \text{ for } x \in \mathbb{R}^3 \setminus \Omega, \tag{3}$$

$$a(x) \in C^3\left(\mathbb{R}^3\right), \tag{4}$$

where $d = const. > 1$ is *a priori* known constant.

Coefficient Inverse Problem (CIP). *Suppose that the coefficient $a(x)$ satisfies (3) and (4). Assume that the function $a(x)$ is unknown in the domain Ω. Determine the function $a(x)$ for $x \in \Omega$, assuming that the following function $g(x,t)$ is known for a single source point position $x_0 \notin \overline{\Omega}$*

$$u(x,t) = g(x,t) \quad \forall (x,t) \in \partial\Omega \times (0,\infty). \tag{5}$$

In our applications we assume that the source point $x_0 \notin \overline{\Omega}$ since we do not want to deal with singularities near the source location. In real applications the assumption $a(x) = 1$ for $x \in \mathbb{R}^3 \setminus \Omega$ means that the function $a(x)$ has a known constant value outside of the medium of interest Ω. The function $g(x,t)$ in (5) models time dependent measurements of the wave field $u(x,t)$ at the boundary of the domain of interest.

3 The Transformation Procedure for the Hyperbolic Case

In this section we show how to reduce our Inverse Problem (CIP) to the Dirichlet boundary value problem for a nonlinear integro-differential equation. First, we take the Laplace transform of the

functions u in the hyperbolic equation (1) to get

$$w(x,s) = \int_0^\infty u(x,t)\mathrm{e}^{-st}dt \quad \text{for } s > \underline{s} = const. > 0, \tag{6}$$

where $\underline{s}$ is a certain number, which we choose in experiments. It is sufficient to choose $\underline{s}$ such that the integral (6) would converge together with corresponding (x,t) derivatives. Thus, we can assume that the number $\underline{s}$ is sufficiently large. The parameter s is called *pseudo frequency*. It follows from (1), (2), and (6) that the function w is the solution of the following problem

$$\Delta w - s^2 a(x) w = -\delta(x - x_0), \ x \in \mathbb{R}^3, \tag{7}$$

$$\lim_{|x|\to\infty} w(x,s) = 0, \tag{8}$$

where the limit in (8) is proven in [5].

We now work only with the function $w(x,s)$. In Theorem 2.7.2 of [5] was shown that $w(x,s) > 0$. Hence, we can consider functions $v(x,s)$ defined as

$$v(x,s) = \frac{\ln w(x,s)}{s^2}. \tag{9}$$

Assuming that the asymptotic behavior in Lemma 2.3 of [5] holds we get the following asymptotic behavior of the function v

$$\left\| D_x^\beta D_s^k v(x,s) \right\|_{C^3(\overline{\Omega})} = O\left(\frac{1}{s^{k+1}}\right), \ s \to \infty, \quad k = 0, 1. \tag{10}$$

Substituting $w = \mathrm{e}^v$ in (7) and noting that the source point $x_0 \notin \overline{\Omega}$ and then dividing the resulting equation for v by s^2, we obtain

$$\Delta v + s^2 (\nabla v)^2 = a(x), \quad x \in \Omega. \tag{11}$$

Denote

$$q(x,s) = \partial_s v(x,s). \tag{12}$$

By (10) and (12) we obtain

$$v(x,s) = -\int_s^\infty q(x,\tau)\, d\tau.$$

We rewrite this integral as

$$v(x,s) = -\int_s^{\overline{s}} q(x,\tau)\, d\tau + V(x,\overline{s}), \tag{13}$$

where the truncation pseudo frequency $\overline{s} > \underline{s}$ is a large number. It is important that $V(x,\overline{s})$ in (13) is not an arbitrary function, but is defined as

$$V(x,\overline{s}) = v(x,\overline{s}) = \frac{\ln w(x,\overline{s})}{\overline{s}^2}, \tag{14}$$

where $w(x,\overline{s})$ is the Laplace transform (6) of the solution of the forward problem (1), (2) at $s := \overline{s}$. The number $\overline{s}$ should be chosen in numerical experiments. We call the function $V(x,\overline{s})$ as the "tail" function and this function is unknown. By (10) and (14) we have that

$$\|V(x,\overline{s})\|_{C^3(\overline{\Omega})} = O\left(\frac{1}{\overline{s}}\right), \quad \|\partial_{\overline{s}} V(x,\overline{s})\|_{C^3(\overline{\Omega})} = O\left(\frac{1}{\overline{s}^2}\right). \tag{15}$$

From above equations follows that the tail is small for large values of $\overline{s}$. Therefore, one can set $V(x,\overline{s}) := 0$. In our recent works [7, 8] we describe alternative approach how this tail function can be approximated in computations.

We now note that in the equation (11) the function $a(x)$ does not depends on the parameter s. Thus, differentiating this equation with respect to s and using (12) and (13), we obtain the following nonlinear integro-differential equation

$$\begin{aligned} &\Delta q - 2s^2 \nabla q \int\limits_s^{\overline{s}} \nabla q(x,\tau)\, d\tau + 2s \left[\int\limits_s^{\overline{s}} \nabla q(x,\tau)\, d\tau\right]^2 \\ &+ 2s^2 \nabla q \nabla V - 4s \nabla V \int\limits_s^{\overline{s}} \nabla q(x,\tau)\, d\tau + 2s(\nabla V)^2 = 0, \quad x \in \Omega. \end{aligned} \tag{16}$$

Conditions(5) and (12) imply that we can set the following Dirichlet boundary condition for the function q

$$q(x,s) = \psi(x,s) \quad \forall (x,s) \in \partial\Omega \times [\underline{s},\overline{s}], \tag{17}$$

where

$$\psi(x,s) = \frac{\partial_s \ln \varphi}{s^2} - \frac{2\ln\varphi}{s^3}$$

and $\varphi(x,s)$ is the Laplace transform (6) of the function $g(x,t)$ in (5).

Assume now that we can solve (16) and find approximations for functions q and V in Ω together with their derivatives $D_x^\alpha q, D_x^\alpha V, |\alpha| \leq 2$. Then the the function $a(x)$ can be found via explicit formula

$$a(x) = \Delta v + \underline{s}^2 (\nabla v)^2, \quad x \in \Omega, \tag{18}$$

where the function v can be obtained via (13).

4 The Layer Stripping Procedure

In this section we describe the layer stripping procedure for the solution of the integro-differential equation (16). To do that we make partition of the pseudo frequency interval $[\underline{s},\overline{s}]$ into N subintervals $\overline{s} = s_0 > s_1 > \cdots > s_N = \underline{s}$ such that

$$\underline{s} = s_N < s_{N-1} < ... < s_1 < s_0 = \overline{s}, s_{i-1} - s_i = h,$$

where h is the step size of every interval and $q(x,s) = q_n(x)$ for $s \in (s_n, s_{n-1}]$. Thus, we approximate the function $q(x,s)$ in (16) by a piecewise constant function with respect to the pseudo frequency s. We also set

$$q_0 \equiv 0. \tag{19}$$

Hence, integrals in (16) can be approximated as

$$\int_s^{\overline{s}} \nabla q(x,\tau)d\tau = (s_{n-1}-s)\nabla q_n(x) + h\sum_{j=0}^{n-1}\nabla q_j(x), s \in (s_n, s_{n-1}). \tag{20}$$

We approximate the boundary condition (17) by a piecewise constant function,

$$q_n(x) = \frac{1}{h}\int_{s_n}^{s_{n-1}} \psi(x,s)\,ds. \tag{21}$$

For every subinterval $(s_n, s_{n-1}], n \geq 1$ we assume that functions $q_j(x),\ j = 1, ..., n-1$, for all previous subintervals are computed. Then we obtain from (16) the following system of approximate equations for the functions $q_n(x)$

$$\begin{aligned}
\widetilde{L}_n(q_n) &:= \Delta q_n - 2\left(s^2 - 2s(s_{n-1}-s)\right)\left(h\sum_{j=1}^{n-1}\nabla q_j\right)\nabla q_n \\
&+ 2\left(s^2 - 2s(s_{n-1}-s)\right)\nabla q_n \nabla V \\
&= 2(s_{n-1}-s)\left[s^2 - s(s_{n-1}-s)\right](\nabla q_n)^2 - 2sh^2\left(\sum_{j=1}^{n-1}\nabla q_j\right)^2 \\
&+ 4s\nabla V\left(h\sum_{j=1}^{n-1}\nabla q_j\right) - 2s|\nabla V|^2, s \in (s_{n-1}, s_n].
\end{aligned} \tag{22}$$

The equation (22) is nonlinear and this equation depends on the parameter s. To involve better stability of the computational process, we add the term $-\varepsilon q_n$ to the left hand side of equation (22). Here, $\varepsilon > 0$ is a small parameter. Then we multiply (22) by the Carleman Weight Function (CWF) of the form

$$\mathcal{C}_{n,\lambda}(s) = \mathrm{e}^{\lambda(s-s_{n-1})}, \quad s \in (s_n, s_{n-1}], \tag{23}$$

and integrate with respect to s over every pseudo frequency interval(s_n, s_{n-1}). In (23) the parameter $\lambda \gg 1$ and it should be chosen in numerical experiments. Finally, we obtain

$$\begin{aligned}
L_n(q_n) &:= \Delta q_n - A_{1,n}\left(h\sum_{j=0}^{n-1}\nabla q_j\right)\nabla q_n + A_{1n}\nabla q_n \nabla V - \varepsilon q_n \\
&= 2\frac{I_{1,n}}{I_0}(\nabla q_n)^2 - A_{2,n}h^2\left(\sum_{j=0}^{n-1}\nabla q_j(x)\right)^2 \\
&+ 2A_{2,n}\nabla V\left(h\sum_{j=0}^{n-1}\nabla q_j\right) - A_{2,n}(\nabla V)^2, n = 1, ..., N,
\end{aligned} \tag{24}$$

with the discretized boundary condition

$$q_n(x) = \psi_n(x) := \frac{1}{h}\int_{s_n}^{s_{n-1}} \psi(x,\, s)\,\mathrm{d}s \approx \frac{1}{2}[\psi(x,\, s_n) + \psi(x,\, s_{n-1})], \quad x \in \partial\Omega. \tag{25}$$

In (24) coefficients can be computed analytically:

$$I_0 := I_0(\lambda, h) = \int\limits_{s_n}^{s_{n-1}} \mathcal{C}_{n,\lambda}(s)\, ds = \frac{1 - e^{-\lambda h}}{\lambda},$$

$$I_{1,n} := I_{1,n}(\lambda, h) = \int\limits_{s_n}^{s_{n-1}} (s_{n-1} - s)\left[s^2 - s(s_{n-1} - s)\right] \mathcal{C}_{n,\lambda}(s)\, ds,$$

$$A_{1,n} := A_{1,n}(\lambda, h) = \frac{2}{I_0} \int\limits_{s_n}^{s_{n-1}} \left(s^2 - 2s(s_{n-1} - s)\right) \mathcal{C}_{n,\lambda}(s)\, ds,$$

$$A_{2,n} := A_{2,n}(\lambda, h) = \frac{2}{I_0} \int\limits_{s_n}^{s_{n-1}} s\mathcal{C}_{n,\lambda}(s)\, ds.$$

In equation (24) the tail function V is also unknown. However, we observe that

$$\frac{|I_{1,n}(\lambda, h)|}{I_0(\lambda, h)} \leq \frac{4\overline{s}^2}{\lambda} \quad \text{for } \lambda h \geq 1. \tag{26}$$

Equation (26) means that by taking $\lambda \gg 1$, we mitigate the influence of the nonlinear term with $(\nabla q_n)^2$ in (24). To solve system (24)–(25), we use following algorithm:

Globally convergent algorithm

- Initialization: set $q_0 \equiv 0$ and compute the first tail function V_0 as described in section 2.9 of [5] and [6].
- For $n = 1, 2, \ldots, N$
  1. Set $q_{n,0} = q_{n-1}$, $V_{n,1} = V_{n-1}$
  2. For $i = 1, 2, \ldots, m_n$
     - Find $q_{n,i}$ by solving (24)–(25) with $V_n := V_{n,i}$.
     - Compute $v_{n,i} = -hq_{n,i} - h\sum_{j=0}^{n-1} q_j + V_{n,i}$.
     - Compute $a_{n,i}$ via discretization of (18) with $a := a_{n,i}$ and $v := v_{n,i}$. Then solve the forward problem (1)–(2) with the new computed coefficient $a := a_{n,i}$, compute $w := w_{n,i}$ and update the tail $V_{n,i+1}$ by (14).
  3. Set $q_n = q_{n,m_n}$, $a_n = a_{n,m_n}$, $V_n = V_{n,m_{n+1}}$ and go to the next frequency interval $[s_{n+1}, s_n]$ if $n < N$. If $n = N$, then stop.

The stopping criteria for iterations m_n and n and step 3 in the above algorithm is derived computationally in [7, 10]. The global convergence theorem was proven in [5, 6].

5 Finite element method for reconstruction

In this section we explain how we can reconstruct the function $a(x)$ of the equation (1) using the variational formulation of equation (7). Suppose that the pair of functions $(V_{n,i}, q_{n,i})$ at step 2 of the globally convergent algorithm is computed. Then using the Finite Difference discretization of (13) we can compute the function $v_{n,i}(x)$ as

$$v_{n,i}(x) = -hq_{n,i}(x) - h\sum_{j=0}^{n-1} q_j(x) + V_{n,i}(x) \quad x \in \Omega. \tag{27}$$

Using (9) we can get

$$v_{n,i}(x) = \frac{\ln w_{a_{n,i}}(x, s_n)}{s_n^2}, \tag{28}$$

and thus

$$w_{a_{n,i}}(x) = \mathrm{e}^{s_n^2 v_{n,i}(x)}.$$

Here, the function $w_{a_{n,i}}(x, s_n)$ is the solution of the following analog of the problem (7), (8)

$$\Delta w_{a_{n,i}} - s_n^2 a_{n,i}(x)\, w_{a_{n,i}} = 0 \text{ in } \Omega, \tag{29}$$

$$\partial_n w_{a_{n,i}} \mid_{\partial\Omega} = f_{n,i}(x), \tag{30}$$

where

$$f_{n,i}(x) = \partial_n \mathrm{e}^{s_n^2 v_{n,i}(x)} \text{ for } x \in \partial\Omega.$$

To find $a_{n,i}$ from (29), we will use the finite element method for the problem (29)–(30). We introduce the finite element trial space V_h, defined by

$$V_h := \{u \in H^1(\Omega) : u|_K \in P_1(K), \forall K \in K_h\},$$

where $P_1(K)$ denotes the set of linear functions on the element K of the finite element mesh K_h. Hence, the finite element space V_h consists of continuous piecewise linear functions in space. To approximate functions $a_{n,i}$ we introduce space of piecewise-linear functions C_h defined by

$$C_h := \{u \in H^1(\Omega) : u|_K \in P_1(K), \forall K \in K_h\},$$

Let us define a L_2 inner product

$$(\alpha, \beta) = \int_\Omega \alpha\beta\, dx.$$

Then the finite element formulation for (29)-(30) reads: Find $a_{n,i} \in C_h, w_{a_{n,i}} \in V_h$ such that for all $v \in V_h$

$$(a_{n,i} w_{a_{n,i}}, v) = -\frac{1}{s_n^2}(\nabla w_{a_{n,i}}, \nabla v) + \frac{1}{s_n^2}(f_{n,i}, v)_{\partial\Omega}. \tag{31}$$

We expand $w_{a_{n,i}}$ in terms of the standard continuous piecewise linear functions $\{\varphi_k\}_{k=1}^N$ in space as

$$w_{a_{n,i}} = \sum_{k=1}^{N} w_{a_{n,i}k} \varphi_k(x), \tag{32}$$

where $w_{a_{n,i}k}$ are the discrete nodal values of the already computed functions $v_{n,i}$ at step 2 of the globally convergent algorithm with the nodal values v_{n,i_k} such that

$$w_{a_{n,i}k} = \mathrm{e}^{s_n^2 v_{n,i_k}(x)} \ \forall x \in \Omega.$$

We substitute expansion (32) in the variational formulation (31) with $v(x) = \varphi_j(x)$, and obtain the following system of discrete equations

$$\sum_{k,j=1}^{N} a_{n,i_k}(w_{a_{n,i}k}\ \varphi_k, \varphi_j) = -\frac{1}{s_n^2}\sum_{k,j=1}^{N} w_{a_{n,i}k}(\nabla\varphi_k, \nabla\varphi_j) + \frac{1}{s_n^2}\sum_{j=1}^{N}(f_{n,i}, \varphi_j)_{\partial\Omega}. \tag{33}$$

The system (33) can be rewritten in the matrix form for the unknown $a_{n,i}$ and known $w_{a_{n,i}}$ as

$$Ma_{n,i} = -\frac{1}{s_n^2} G w_{a_{n,i}} + \frac{1}{s_n^2} F. \tag{34}$$

Here, M is the block mass matrix in space, G is the stiffness matrix corresponding to the gradient term, F is the load vector. At the element level the matrix entries in (34) are explicitly given by:

$$M_{k,j}^K = (w_{a_{n,i}k}\ \varphi_k, \varphi_j)_K, \tag{35}$$

$$G_{k,j}^K = (\nabla\varphi_k, \nabla\varphi_j)_K, \tag{36}$$

$$F_j^K = (f_{n,i}, \varphi_j)_K. \tag{37}$$

To obtain an explicit scheme for the computation of the coefficients $a_{n,i}$, we approximate M by the lumped mass matrix M^L in space. This matrix is obtained as the diagonal approximation of the mass matrix M: diagonal elements of M^L are obtained as the row sum of elements in M. Thus, we get the following equation for the explicit computation of the function $a_{n,i}$ in (29):

$$a_{n,i} = -\frac{1}{s_n^2}(M^L)^{-1} G w_{a_{n,i}} + \frac{1}{s_n^2}(M^L)^{-1} F. \tag{38}$$

6 Numerical experiments in 2D

In this section we present the reconstruction of wave speed function $a(x)$ at different values of pseudo frequency s for the the case when the measured function $u_\sigma(x,t)$ is known inside the domain of interest. Measuring of the field internally is allowed in some cases of medical imaging: for example, in medical resonance elastic imaging [2].

6.1 Data simulation in 2d

For generation of data to solve our CIP, we first solve the forward problem for the wave equation with known value of a wave speed inside our domain of interest. Let us define by G the computational domain where we compute the forward problem.

We simulate the data for the inverse problem using the software package WavES [12]. To do that we solve the forward problem via the hybrid finite element/finite difference (FEM/FDM) method of [3]. In this method the computational domain G is split in two subdomains, $G = G_{FDM} \cup G_{FEM}$, see Figure 1 for these subdomains. We use structured mesh with FDM in G_{FDM} and non-structured mesh and FEM in $G_{FEM} = \Omega$. The computational domain $G_{FEM} =$

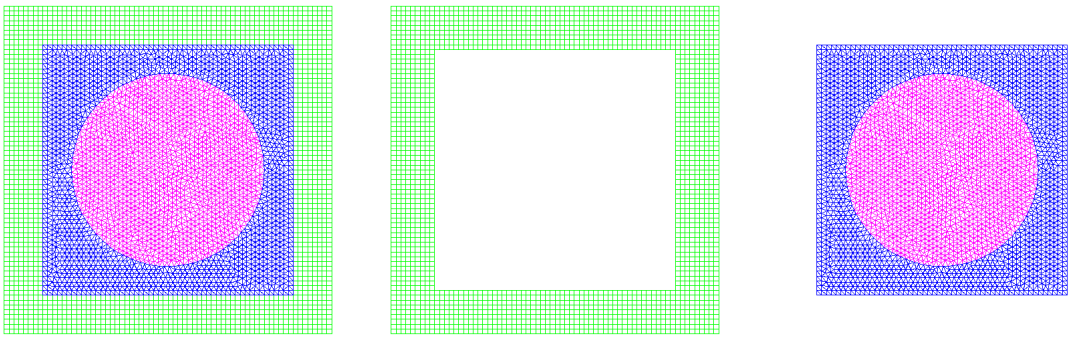

a) $G = G_{FEM} \cup G_{FDM}$ b) G_{FDM} c) $G_{FEM} = \Omega$

Figure 1: *a) Geometry of the hybrid mesh. This is a combination of the quadrilateral finite difference mesh in the subdomain G_{FDM} presented on b), and the finite element mesh in the inner domain $G_{FEM} = \Omega$ presented on c). The solution of the inverse problem is computed in $G_{FEM} = \Omega$. We use software package WavES [12] to compute hybrid solution on these meshes.*

Ω is also decomposed into two domains $G_{FEM} = G_{circ} \cup (G_{FEM} \setminus G_{circ})$, where G_{circ} is the circular FEM domain where we search tumor-like inclusions. The boundary of the rectangle G is $\partial G = \partial G_1 \cup \partial G_2 \cup \partial G_3$. Here, ∂G_1 and ∂G_2 are respectively top and bottom sides of the largest rectangle of Figure 1, and ∂G_3 is the union of left and right sides of this rectangle. The space mesh in Ω consists of triangles and it consists of squares in G_{FDM}, with the mesh size $\tilde{h} = 0.02$ in the overlapping regions.

We generate the data via solution of the following forward problem

$$
\begin{aligned}
a(x)\, u_{tt} - \Delta u &= 0 \quad \text{in } G \times (0,T), \\
u(x,0) = 0,\ u_t(x,0) &= 0, \ \text{in } G, \\
\partial_n u\big|_{\partial\Omega_1} &= f(t) \ \text{ on } \partial G_1 \times (0,t_1], \\
\partial_n u\big|_{\partial\Omega_1} &= \partial_t u \text{ on } \partial G_1 \times (t_1,T), \\
\partial_n u\big|_{\partial G_2} &= \partial_t u \text{ on } \partial G_2 \times (0,T), \\
\partial_n u\big|_{\partial\Omega_3} &= 0 \text{ on } \partial G_3 \times (0,T).
\end{aligned} \tag{39}
$$

The plane wave $f(t)$ is given by

$$
f(t) = \begin{cases} \sin \omega t & \text{for } t \in (0, \frac{2\pi}{\omega}] = (0,t_1], \\ 0 & \text{for } t \in \left(\frac{2\pi}{\omega}, T\right) \end{cases} \tag{40}
$$

and is initialized at the top boundary ∂G_1 of the computational domain G of Figure 1. The plane wave propagates downwards into G and is absorbed at the bottom boundary ∂G_2 for all times $t \in (0,T)$. In addition, it is also absorbed at the top boundary ∂G_1 for times $t \in (t_1,T)$. We use first-order absorbing boundary conditions [9]. In our tests we took $\omega = 20$ and $T = 2$ in (40), see some simulations of the forward problem on Figure 2. When solving the inverse problem, we assume that the coefficient $a(x)$ is unknown in the circle $G_{circ} \subset G$ and has a known constant value $a(x) = 1$ in $G \setminus \Omega$ and in $G_{FEM} \setminus G_{circ}$, see Figure 1.

The trace $g(x,t)$ of the solution $u(x,t)$ of the wave equation is recorded inside the circle G_{circ} where we want to reconstruct the function $a(x)$. Next, the coefficient $a(x)$ is forgotten,

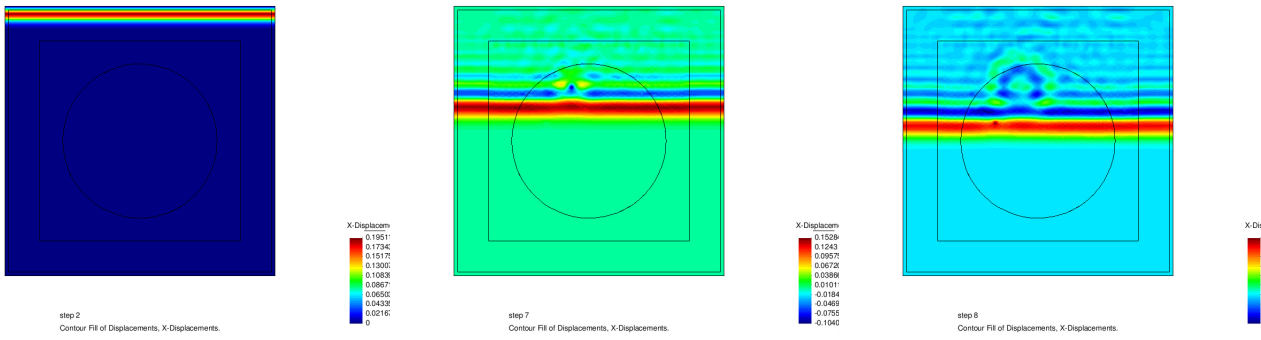

a) $t = 0.2$ b) $t = 0.7$ c) $t = 0.8$

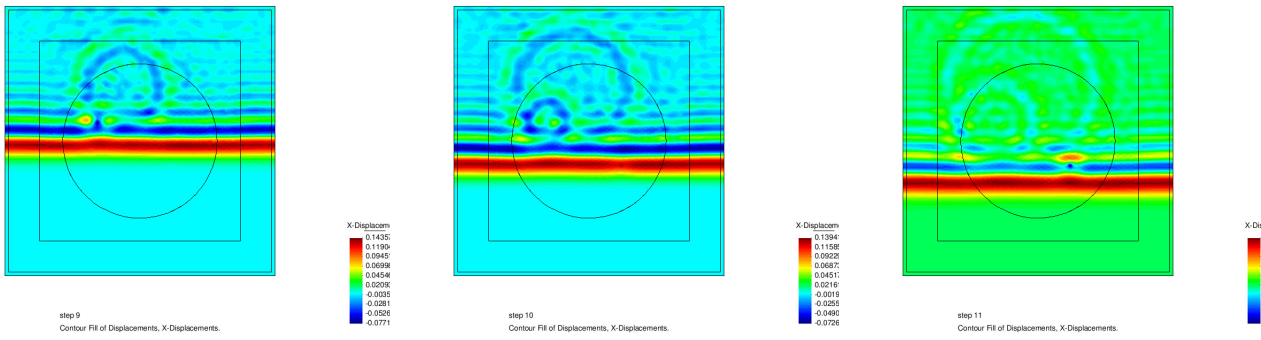

d) $t = 0.9$ e) $t = 1.0$ f) $t = 1.1$

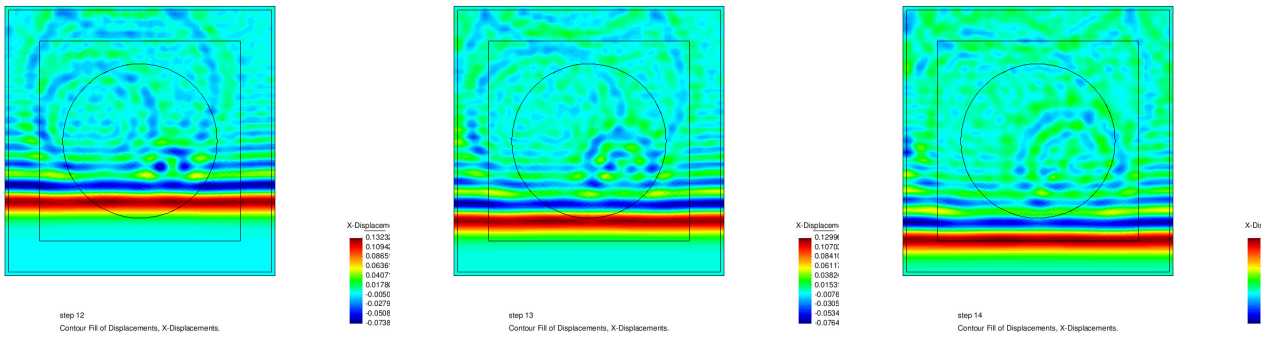

g) $t = 1.2$ h) $t = 1.3$ i) $t = 1.4$

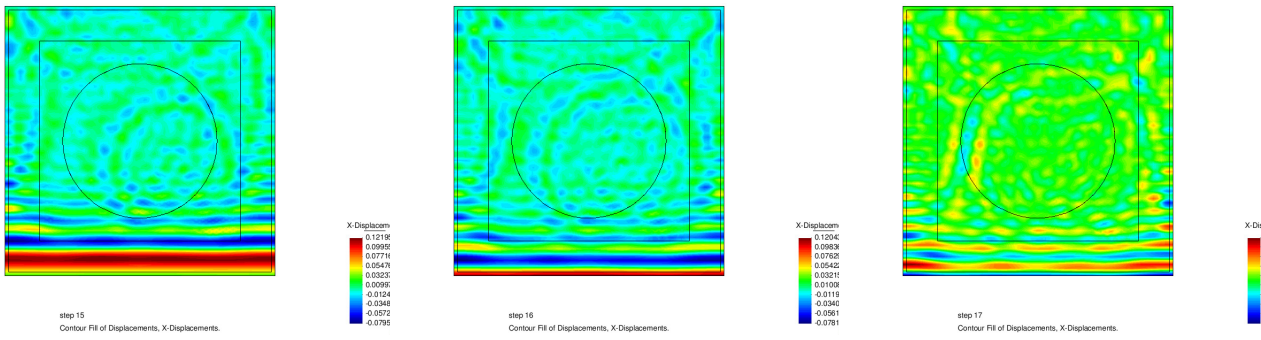

j) $t = 1.5$ k) $t = 1.6$ l) $t = 1.7$

Figure 2: *Isosurfaces of the computed solution* $u(x, t)$ *of the wave equation in* G *at different times* t *with the plane wave initialized at the front boundary of the domain* G*. Test was computed in time* $t = [0, 2]$ *with time step* $\tau = 0.001$*. Software package WavES [12] is used for the numerical simulation of this solution.*

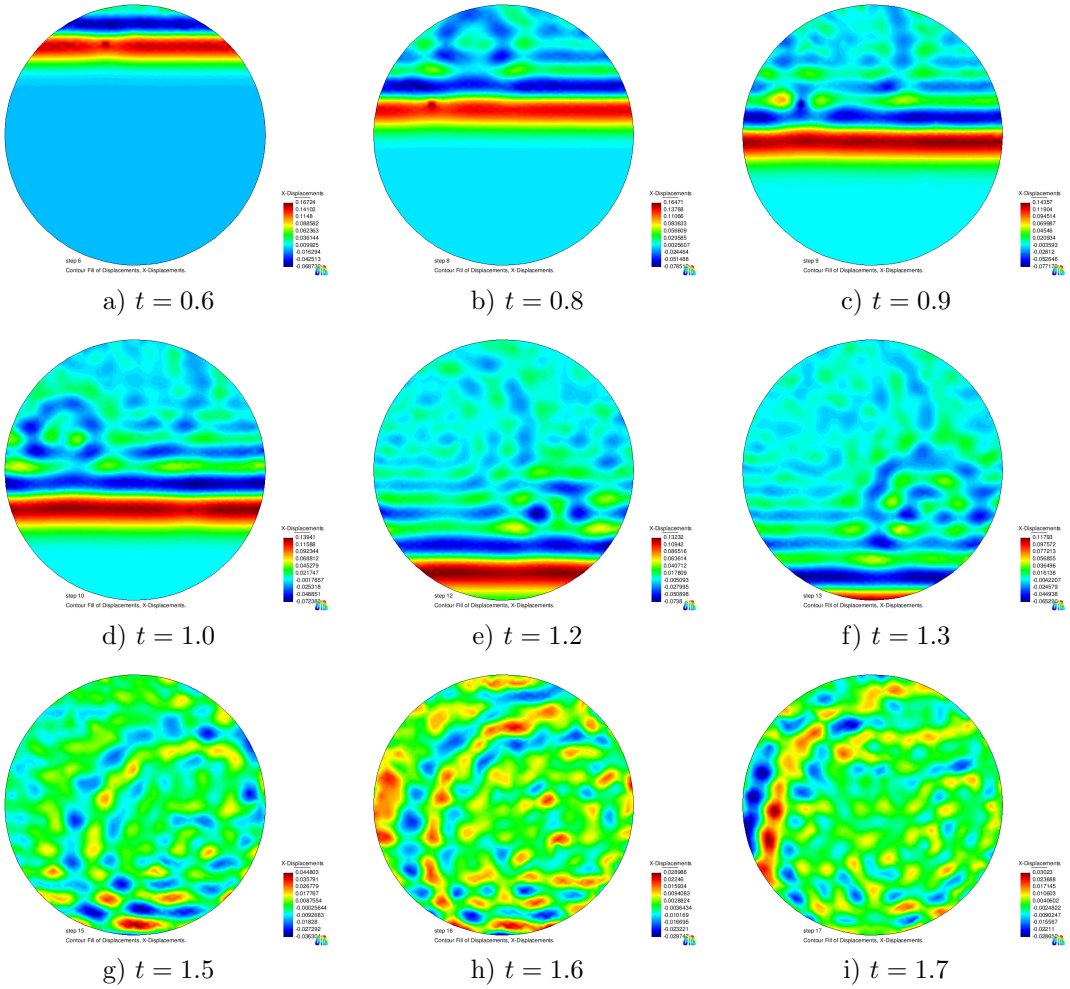

a) $t = 0.6$ b) $t = 0.8$ c) $t = 0.9$

d) $t = 1.0$ e) $t = 1.2$ f) $t = 1.3$

g) $t = 1.5$ h) $t = 1.6$ i) $t = 1.7$

Figure 3: *Extracted isosurfaces of the computed solution* $u(x,t)$ *of Figure 2 in* G_{circ}.

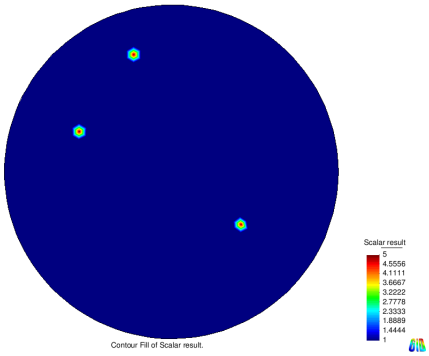

a) exact function $a(x)$

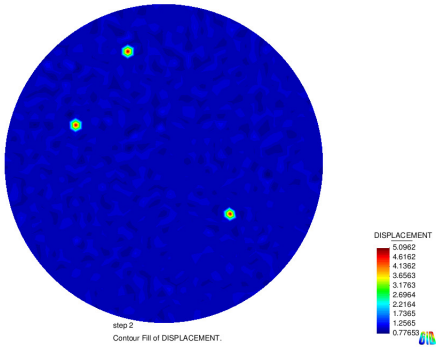

b) computed at $s = 19$

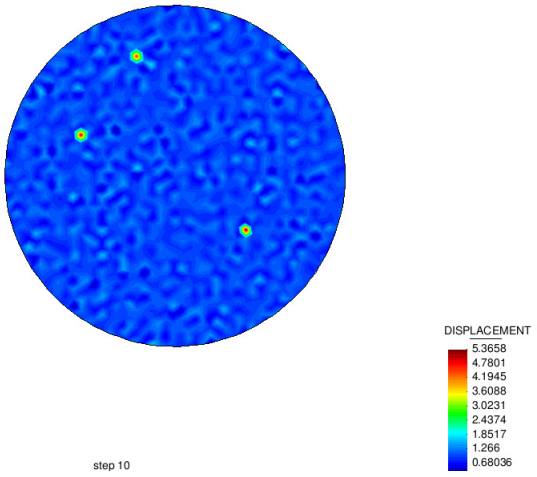

c) computed at $s = 10$

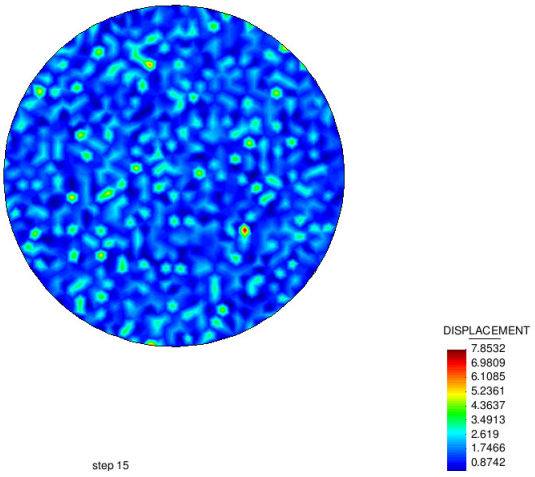

d) computed at $s = 5$

Figure 4: *Test 1: a) The exact location of tumors. b), c), d) The reconstructed wave speed function $a(x)$ at different values of pseudo frequency s for the the case when the measured function $u_\sigma(x,t)$ is known inside the domain of interest. On b) maximal reconstructed values of this function are* 5.09 *in three small tumor-like targets. The reconstructed $a(x) = 1$ outside of imaged targets what corresponds to the background medium. Reconstruction presented on b) is highly accurate: compare with figure a) where values of the exact function $a(x)$ inside tumor-like inclusions are $a(x) = 5$. However, on d) we observe that at pseudo frequency $s = 5$ the image is deteriorated.*

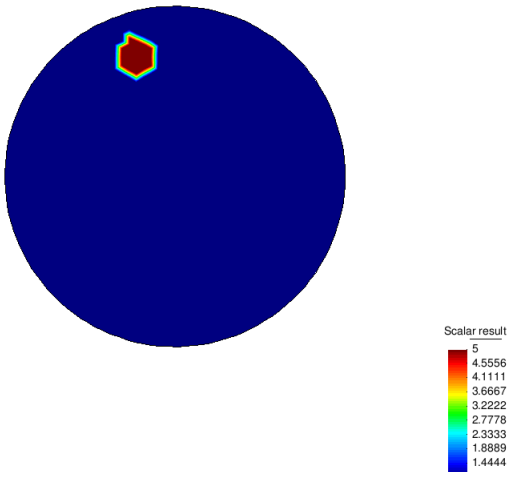

a) exact function $a(x)$

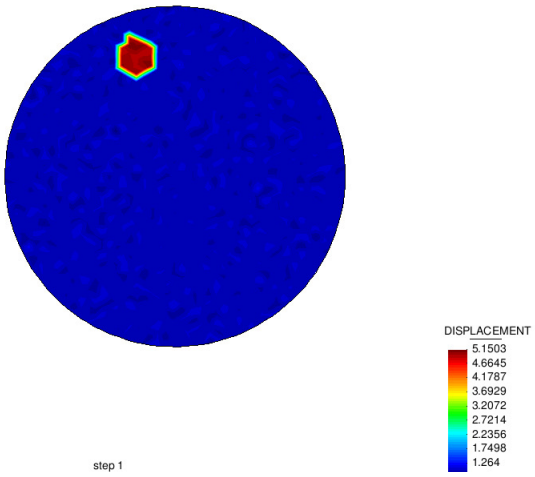

b) computed at $s = 19$

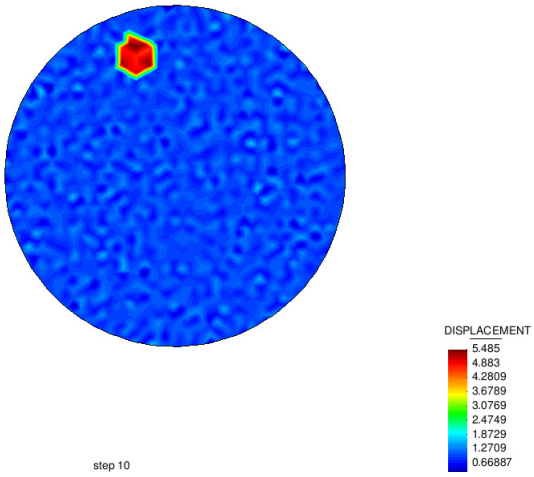

c) computed at $s = 10$

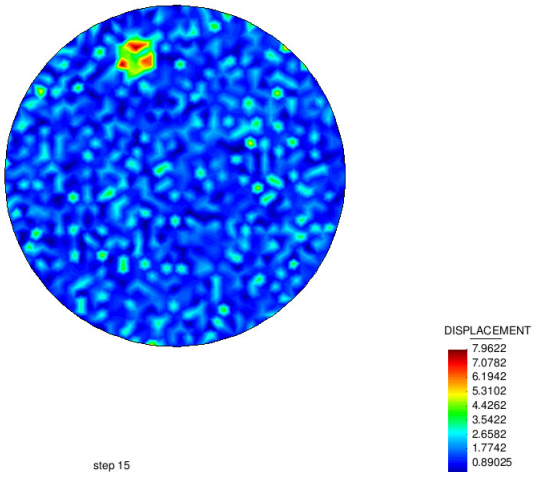

d) computed at $s = 5$

Figure 5: *Test 2: a) The exact location of tumor. b), c), d) The reconstructed wave speed function $a(x)$ at different values of pseudo frequency s for the the case when the measured function $u_\sigma(x,t)$ is known inside the domain of interest. On b) reconstructed maximal values of this function are* 5.15 *in tumor-like target and $a(x) = 1$ outside of imaged target what corresponds to the background medium. The image presented on b) is highly accurate: compare with figure on a) where the function $a(x)$ in the exact tumor-like target has value* 5*. However, on d) we observe that the image is deteriorated at pseudo frequency $s = 5$.*

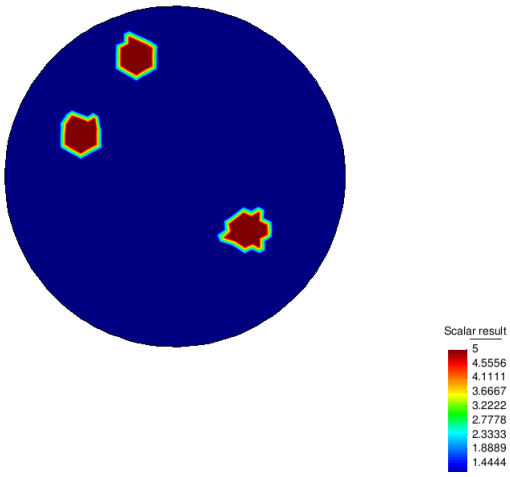

a) exact function $a(x)$

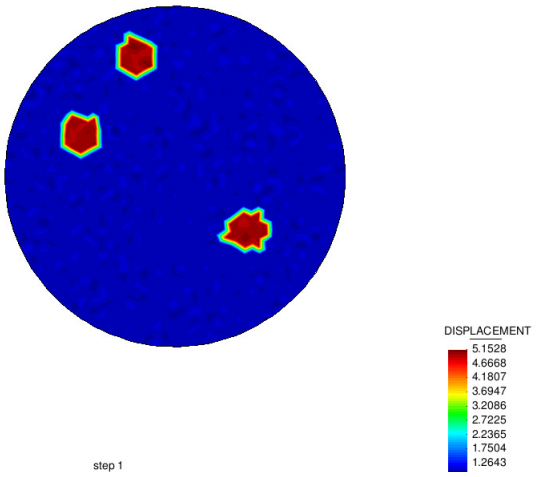

b) computed at $s = 19$

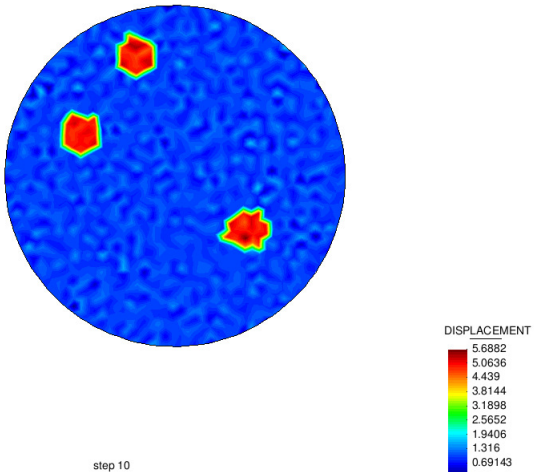

c) computed at $s = 10$

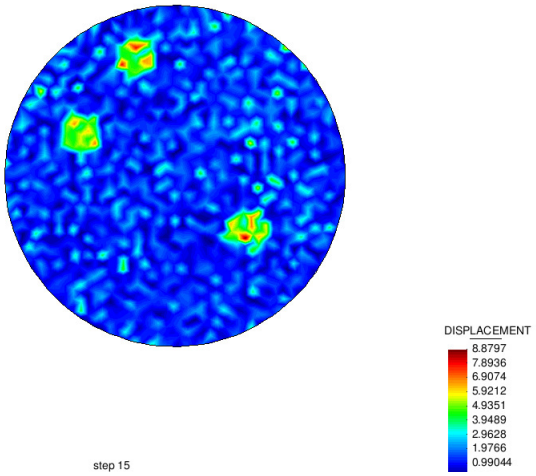

d) computed at $s = 5$

Figure 6: *Test 3: a) The exact location of tumors. b), c), d) The reconstructed wave speed function $a(x)$ at different values of pseudo frequency s. On b) maximal reconstructed values of this function are* 5.15 *in tumor-like targets and $a(x) = 1$ outside of imaged targets what corresponds to the background medium. The image is highly accurate: compare with exact image on a) where maximal values of the exact function are* 5*. Again, on d) we observe that the image is deteriorated at pseudo frequency $s = 5$.*

and our goal is to reconstruct this coefficient for $x \in \Omega$ from the data $\psi(x,s)$ which are obtained after Laplace transform of the data $g(x,t)$. We impose 5% of additive noise to the data $u(x,t)$ to get the measured function $u_\sigma(x,t)$:

$$u_\sigma(x_i,t_j) = u(x_i,t_j)[1 + \alpha_j(u_{max}(x_i,t_j) - u_{min}(x_i,t_j))\sigma]. \tag{41}$$

Here, $u(x_i,t_j)$ is the solution of the problem (39) at the mesh point x_i and time moment $t_j \in (0,T)$, α_j is a random number on the interval $[-1,1]$, $u_{max}(x_i,t_j)$ and $u_{min}(x_i,t_j)$ are maximal and minimal values of the computed solution $u(x_i,t_j)$, respectively, and $\sigma = 0.05$ is the level of the noise.

6.2 Test 1

We model the problem of imaging of three point-like tumor inclusions of Figure 4-a) as an CIP for the scalar wave equation. We set the dimensionless computational domain G as

$$G = (-0.7, 0.7) \times (-0.7, 0.7) \tag{42}$$

and the dimensionless domain $G_{FEM} = \Omega$ as

$$\Omega = (-0.52, 0.52) \times (-0.52, 0.52). \tag{43}$$

Our domain of interest $G_{circ} \subset G$ where we solve our CIP and search for tumors, has the center at the point with coordinates $(0,0)$ and the radius $r = 0.4$. We model our three point-like tumors (p_1, p_2, p_3) to be located at points of the domain G_{circ} with coordinates

$$\begin{aligned} &p_1(x_1,y_1) : x_1 = -0.090234, y_1 = 0.280903, \\ &p_2(x_2,y_2) : x_2 = -0.221014, y_2 = 0.096346, \\ &p_3(x_3,y_3) : x_3 = 0.166988, y_3 = -0.126124. \end{aligned} \tag{44}$$

Medical experiments show that the relation of the function $a(x)$ in cancerous tumors to the healthy tissue is ≈ 5. Thus, we consider the following relative values of the function $a(x)$ in our tests

$$a(x) = \begin{cases} 1 & \text{healthy tissue}, \\ 5 & \text{cancerous tumors}. \end{cases} \tag{45}$$

In Figure 4-b) we present reconstruction of three tumor-like inclusions of Figure 4-a). We use globally convergent algorithm of section 4 to get reconstructed function $a(x)$ of Figures 4-b), c), d). Discrete values $a_{n,i}$ at every point i of the computational domain G_{FEM} are obtained using formula (38). We took pseudo frequency interval $s = [1,19]$ and divided it into subintervals with the step size $\delta s = 1$ for every interval.

Using Figures 4-b), c) we observe that we get almost perfect reconstruction when pseudo frequency s is taken on the interval $s = [8;19]$. However, for pseudo frequencies on the interval $s = [1;7]$ we obtain reconstructed function $a(x)$ similar to the one obtained on Figure 4-d). We observe that the image of Figure 4-d) is deteriorated for this value of pseudo frequency.

6.3 Test 2

This is the same test as the Test 1 of section 6.2, only the goal is image one big tumor-like inclusion of Figure 5-a).

Results are very similar to results of Test 1. On Figures 5-b), c) we observe almost perfect reconstruction when pseudo frequency s is taken as $s = 10$ and $s = 19$. Our numerical tests show that on the interval of pseudo frequencies $s = [8; 19]$ we get reconstruction similar to the exact one of figure 5-b). However, for pseudo frequencies on the interval $s = [1; 7]$ we obtain reconstructed function $a(x)$ similar to the one obtained on Figure 5-d). We observe that the image of Figure 5-d) is deteriorated for this value of pseudo frequency.

6.4 Test 3

This is the same test as the Tests 1 and 2 above, only the goal is image 3 big tumor-like inclusions of Figure 6-a). Results of reconstruction are similar to results of Tests 1 and Test 2 and are presented on Figure 6-b), c), d).

7 Summary

We have applied a finite element method inside the approximately globally convergent method of [5] for explicit reconstruction of the coefficient in the hyperbolic equation. In our numerical tests we have used the measured function which was known inside the domain of interest. This is possible, for example, in the case of magnetic resonance elastography (MRE) which allows measure field internally [2, 11]. In this work we considered the simplified model problem described by the acoustic wave equation instead of the elastic one. The elastodynamics system is planned to be considered in our future research. Results of our numerical examples show quantitative and accurate reconstruction of small tumor-like inclusions.

Acknowledgments

This research was supported by the Swedish Research Council.

References

[1] M. Asadzadeh and L. Beilina, A posteriori error analysis in a globally convergent numerical method for a hyperbolic coefficient inverse problem, *Inverse Problems*, 26, 115007, 2010.

[2] P. E. Barbone and J. C. Bamber, Quantitative elasticity imaging: what can and cannot be inferred from strain images, *Phys.Med.Biol.*, 47, pp.2147-2164, 2002.

[3] L. Beilina, K. Samuelsson and K. hlander, Efficiency of a hybrid method for the wave equation. In *International Conference on Finite Element Methods*, Gakuto International Series Mathematical Sciences and Applications, Gakkotosho CO., LTD, 2001.

[4] L. Beilina and C. Clason, An adaptive hybrid FEM/FDM method for an inverse scattering problem in scanning acoustic microscopy, *SIAM Sci.Comp.*, V.28, I.1, pp.382–402, 2006.

[5] L. Beilina and M.V. Klibanov, *Approximate Global Convergence and Adaptivity for Coefficient Inverse Problems*, Springer, New York, 2012.

[6] L. Beilina and M.V. Klibanov, A new approximate mathematical model for global convergence for a coefficient inverse problem with backscattering data, J. Inverse and Ill-Posed Problems, 20, pp.513–565, 2012.

[7] L. Beilina, Nguyen Trung Thành, M. V. Klibanov, M. A. Fiddy, Reconstruction from blind experimental data for an inverse problem for a hyperbolic equation, *Inverse Problems* 30, 025002, doi:10.1088/0266-5611/30/2/025002, 2014.

[8] L. Beilina, Nguyen Trung Thành, M. V. Klibanov, J.Bondestam Malmberg, Reconstruction of shapes and refractive indices from backscattering experimental data using the adaptivity, *Inverse Problems* 30, 105007, 2014.

[9] B. Engquist and A. Majda, Absorbing boundary conditions for the numerical simulation of waves *Math. Comp.* 31, 629–651, 1977.

[10] Nguyen Trung Thành, L. Beilina, M. V. Klibanov and M. A. Fiddy, Reconstruction of the refractive index from experimental backscattering data using a globally convergent inverse method, *SIAM J. Scientific Computing*, 36 (3), pp.273–293, 2014.

[11] Wall, David J.N.; Olsson, Peter; van Houten, Elijah E. W., On an inverse problem from magnetic resonance elastic imaging, *SIAM Journal on Applied Mathematics*, 2011.

[12] WavES, the software package, http://www.waves24.com